Nuclear Instruments and Methods in Physics Research A 1060 (2024) 169022

Contents lists available at ScienceDirect

Nuclear Inst. and Methods in Physics Research, A

journal homepage: www.elsevier.com/locate/nima

Investigation of radiation emitted by sub GeV electrons in oriented scintillator crystals

L. Bandiera [b], R. Camattari [b], N. Canale [b], D. De Salvador [c,d], V. Guidi [a,b], P. Klag [f], W. Lauth [f], A. Mazzolari [b], R. Negrello [a,b,*], G. Paternò [b], M. Romagnoni [b], F. Sgarbossa [d,c], M. Soldani [a,b], A. Sytov [b], V.V. Tikhomirov [e]

[a] Department of Physics and Earth Science, University of Ferrara, Via Saragat 1, Ferrara, 44122, Italy
[b] INFN Section of Ferrara, Via Saragat 1, Ferrara, 44122, Italy
[c] Department of Physics, University of Padua, Via Marzolo 8, Padua, 35131, Italy
[d] INFN Laboratori Nazionali di Legnaro, Viale dell'Università 2, Legnaro, 35020, Italy
[e] Institute for Nuclear Problems, Belarusian State University, Bobruiskaya 11, Minsk, 220030, Belarus
[f] Institut für Kernphysik der Universität Mainz, Mainz, 55099, Germany

ARTICLE INFO

Keywords:
Channeling
Scintillator
Radiation
Detector

ABSTRACT

The research investigates coherent interactions between sub-GeV electrons and oriented scintillator crystals, leading to enhanced electromagnetic (EM) radiation. Experiments at Mainz Mikrotron (MAMI) involved PWO, BGO, and CsI crystals oriented along ⟨100⟩, ⟨111⟩, and ⟨100⟩ axes, respectively. Enhanced radiation emission was observed when the beam was aligned with crystal axes, especially in BGO and CsI for the first time. These findings are crucial for innovative detectors using oriented crystal scintillators, amplifying EM processes along specific crystallographic directions. Potential applications include ultra-compact, highly sensitive electromagnetic calorimeters for high-energy physics and astroparticles, as well as high-performance gamma detectors for nuclear physics and medical imaging.

1. Introduction

In particle physics, inorganic scintillator crystals are commonly used as gamma, charged particle detectors, as well as electromagnetic (EM) calorimeters. As an example of a state-of-the-art crystal EM calorimeter, the ECAL for the Compact Muon Solenoid (CMS) experiment at CERN, consists of 80 000 crystals of lead tungstate ($PbWO_4$, abbreviated PWO). Bismuth Germanate crystals ($Bi_4Ge_3O_{12}$, abbreviated BGO), are used in nuclear medicine for tumour diagnosis through Positron Emission Tomography (PET) or in the Dark Matter Particle Explorer (DAMPE). In many space-borne experiments, such as the Fermi Gamma-ray Space Telescope, a Cesium Iodide (CsI) crystal e.m. calorimeter is one of the key sub-detectors, designed to perform measurements over a wide energy range,from a few GeV up to several TeV. There is a property not yet exploited in these applications: the interaction between charged particles and a crystalline medium, presenting significant variations depending on the angle of particle trajectories and crystal orientation [1,2]. Random orientation results in ordinary multiple scattering, producing an ordinary bremsstrahlung spectrum. When particles are closely aligned with a crystal plane or axis, they experience the interaction of the periodic potential of the crystal electric field averaged over the coordinate(s) parallel to the atomic plane or string. Negatively charged particles are bound to atomic planes or strings, while positively charged particles scatter between nearby axes, leading to channeling effects and specific radiation emission. The so-called Channeling Radiation (CR) typically displays a dipole feature at sub-GeV energies [3,4], increasing in intensity to the low-energy region of the bremsstrahlung spectrum [5–7]. In contrast, a synchrotron-like spectrum is formed at a few-GeV or higher, with a further increase in the energy of the enhanced spectral components [8–11]. The angular acceptance of the channeling effect, the Lindhard angle, can be calculated using the following formula:

$$\theta_C = \sqrt{\frac{2U_0}{pv}} \tag{1}$$

where U_0 is the depth of the averaged atomic potential calculated for the specific axis/plane, while pv for relativistic particles is basically its energy. If a PWO crystal is considered, along ⟨100⟩ axis, the value of U_0 is approximately 470 eV, therefore, if incident particle energy is about 1 GeV, the value for the Lindhard angle is about 1 mrad. At

* Corresponding author at: Department of Physics and Earth Science, University of Ferrara, Via Saragat 1, Ferrara, 44122, Italy.
E-mail addresses: bandiera@fe.infn.it (L. Bandiera), riccardo.negrello@unife.it (R. Negrello).

https://doi.org/10.1016/j.nima.2023.169022
Received 31 October 2023; Received in revised form 5 December 2023; Accepted 11 December 2023
Available online 12 December 2023

Table 1
Sample parameters.

Sample material	PWO	BGO	CsI
Lateral size (mm^2)	8 × 8	10 × 10	15 × 15
Thickness (mm)	0.5	0.1	1
Main surface	(100)	(100)	(100)
Axes	[100]	[111]	[100]

higher particle energies, the so-called Strong Field regime is achieved when $\frac{\gamma E}{E_0} > 1$, where E is the electric field along the axis in the laboratory frame, and $E_0 \approx 1.32 \times 10^{18}$ V/m is the Schwinger QED critical field, above which nonlinear effects occur in vacuum. The electromagnetic field to which charged particles are subjected in their Lorentz frames is boosted by a factor γ. In comparison to the random condition, the Bremsstrahlung spectrum, the interactions with the crystalline structure in the Strong Field regime enhance the emission of synchrotron radiation, which exhibits high intensity in the hard-photon component and a larger radiative energy loss compared to incoherent Bremsstrahlung. The present study was conducted at energies that prevent the Strong Field effect, to verify and quantify the increase in radiation produced, even at low energies, for these high-Z scintillator crystals when specific crystal axes are aligned with the incident beam compared with the random (amorphous) orientation case. The aim of our study is to demonstrate the suitability of the crystalline materials PWO, BGO and CsI for coherent effect applications, highlighting their potential as gamma emitters in crystal-based light sources [12–14]. These discoveries present also the possibility to develop more effective gamma detectors, suitable for applications in particle and astroparticle physics [15–17]. Here, experimental results of enhancement of radiation production due to coherent effects in PWO, CsI, and BGO scintillator crystals, for the [100], [111], and [100] axes respectively, are shown. The data were collected at the Mainz Microtron (MAMI) facility, by aligning the crystal axes with a electron beam tuned to 855 MeV.

2. Characterization

The scintillator crystals, with features reported in Table 1, were tested through hard X-ray at the ID11 and BM05 beamlines at the European Synchrotron Radiation Facility (ESRF) of Grenoble (France) to measure their lattice quality. Indeed, the crystallographic perfection is mandatory to exploit axial effect for the enhancement of electron beam interaction in an oriented scintillator crystal. The performed characterizations are described here below.

2.1. Hard X-ray diffraction

A highly monochromatic and quasi-parallel X-ray beam 50 × 50 μm wide was tuned to 140 keV energy. The monochromaticity was of the order of $\Delta E/E = 10^{-3}$. The beam traversed the crystal thickness. The first measurement consisted in a photographic plate that was impressed with the X-rays that were diffracted by the sample while it was rotated about a vertical axis, perpendicular to the X-ray beam. This measure was used for a preliminary check of the crystallographic orientation and quality of the samples. The results are shown in Fig. 1.

Subsequently, the nearest diffraction points were analyzed with the same beam via Rocking Curves (RC), *i.e.* by recording the diffracted beam intensity while the crystal was being oriented around the position where Bragg condition was satisfied. The diffraction RC was recorded by a photo-diode as a function of the beam glancing angle. The samples were set far enough from the detectors to allow sufficient separation of diffracted and transmitted beams. The results are shown in Fig. 2. As can be seen, the values of Full Width at Half Maximum (FWHM) of the RCs, which are a good indicator of the mosaicity of the samples and then of their crystalline quality, is very low, namely 0.088, 0.081, and

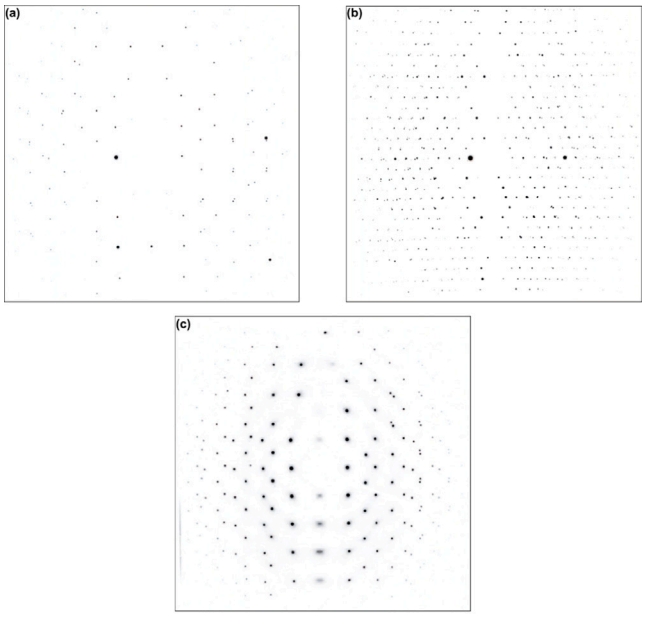

Fig. 1. Photographic plate measurements: (a) PWO; (b) BGO; (c) CsI. Diffraction points showing the crystalline structure.

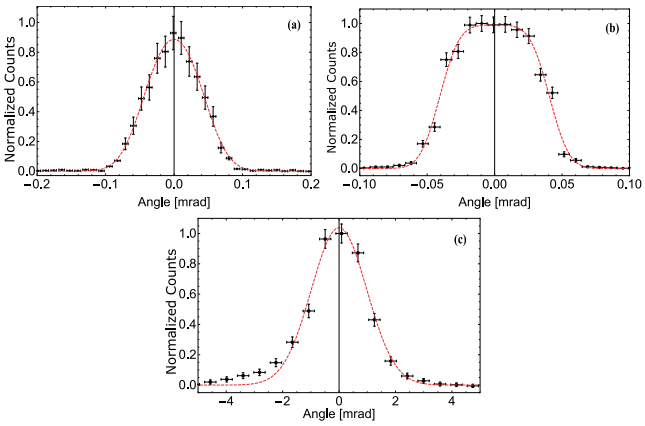

Fig. 2. RC measurements. (a) PWO; (b) BGO; (c) CsI. The dashed red lines are the fitted function to find the mosaicity of the samples.

2.3 mrad for the PWO, the BGO, and the CsI sample, respectively. The FWHM values have been found by fitting the RCs (red dashed lines in the figures).

2.2. X-ray topography

The crystalline quality of the scintillator samples were also measured through monochromatic X-ray topography at the BM05 beamline of ESRF. In particular, the samples were analyzed through Rocking Curve Imaging in reflection mode (Bragg geometry).

The beam was set to 20 keV with a monochromaticity of the order of $\Delta E/E = 10^{-4}$, and was 10 × 10 mm wide. The sample had to be rotated around the position where Bragg condition was satisfied. The detector was a FReLoN camera with pixel size of 5 × 5 μm. The image size was 100 × 100 mm, however in case of reflection the image size corresponds to 10 mm in the horizontal direction and 10 mm/sin(Bragg angle) in the vertical direction. Thus, the images turned out to be compressed along the vertical direction. The sample surfaces were analyzed by stitching all the measurements. The result of the measurement consisted in a map of the sample surface. In particular, for every point of

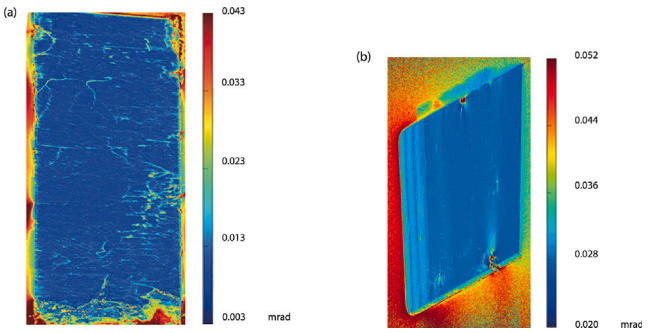

Fig. 3. X-ray topography. (a) PWO; (b) BGO.

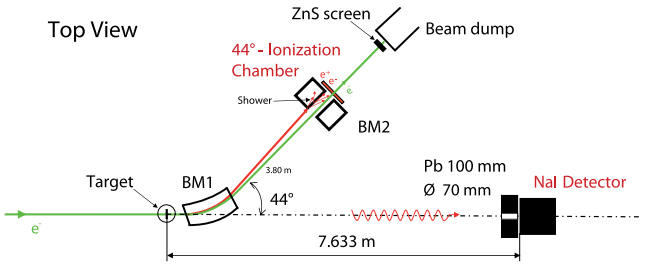

Fig. 4. MAMI experimental setup, top view. Photon spectra are detected with a NaI detector. The detector is shielded by a 100 mm thick lead wall with a 70 mm opening for the photons. The 44°-ionization chamber, filled with air at standard pressure, is employed to detect crystal alignment. Downstream the crystal target, the beam is deflected horizontally by the 44° bending magnet BM1 and vertically by a 7.2° bending magnet BM2. Showers are produced by the electrons that leave the nominal direction due to scattering in the target (in red). Just in front of the beam dump, the beam spot can be monitored with a ZnS luminescent screen which is viewed by a CCD camera.

the surface, a RC was recorded. Fig. 3 consists in a map of all the FWHMs of the corresponding RCs. The sample surface turned out to be quite homogeneous, with a mosaicity compatible with that found during RC measurements. Some superficial defect is visible in red, where the mosaicity is increased. Unfortunately, the measurement of X-ray topography could not be performed on the CsI sample, probably because its hygroscopic nature ruined its surface enough to not allow investigation of its surface.

3. Experimental method

After the characterization that attested the high crystallographic quality of the scintillator samples, an experiment to verify the increase of interaction probability between an electron beam and the samples in case of axial alignment was performed at the Mainz Microtron (MAMI) at Mainz, Germany. The experimental setup is shown in Fig. 4 (see [18,19]). The low emittance electron beam available at MAMI was tuned to 855 MeV, resulting in a pencil beam with dimensions of 100×100 μm^2 and small angular divergence, boasting an emittance of just 1 $\mu rad * mm$. The crystals were mounted on a goniometer with which rotations around two axis could be accomplished. The electron beam traversed the scintillator sample through its thickness, along specific axis (see Table 1), thus generating channeling radiation. Then, the photons emitted by the electrons inside the sample were separated by the charged beam through a bending magnet (BM1) and after 7.633 m arrived at a 25.4×25.4 cm^2 NaI scintillator detector. An aperture of 70-mm diameter in the lead shield that surrounded the detector permitted the collection of a portion of the emitted photons, resulting in a collimator aperture of 4.63 mrad, *i.e.*, equal to ~7.8 times the $1/\gamma$ angle, to collect most of the emitted photons.

The alignment of the electron beam with the axes of the crystalline target was accomplished through a 44°-ionization chamber behind the

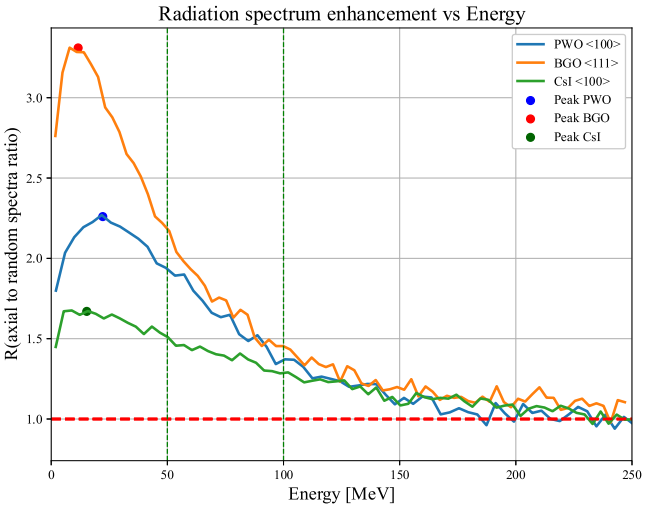

Fig. 5. Experimental data collected at MAMI, depicting the ratios R of radiation spectra along the axis with respect to random, obtained for each crystal. Enhancement peaks are denoted by colored dots, with green dashed vertical lines indicating the reference energies at 50 and 100 MeV. The amorphous spectrum line, normalized to 1, is represented by the red dashed line.

bending magnet BM2. This chamber is sensitive to the charged particles of e.m. showers which are produced by the electrons that leaved the nominal beam direction due to scattering or after emission of multi-MeV photons in the target crystal. Thus, when the crystal axes were aligned with the electron beam, a clear signal was visible via the ionization chamber. Finally, beam-off background has been subtracted from the obtained spectra. In order to measure the radiation spectrum, a calibration of the NaI detector was performed by using the natural radioactive isotopes ^{40}K (1.461 MeV) and ^{208}Tl-^{228}Th (2.6146 MeV). The measured samples were a PWO, a BGO, and a CsI scintillator crystals.

4. Results and discussion

The investigation focused on analyzing the spectrum of electromagnetic processes in the axially oriented samples. This spectrum was generated by the interaction between particles and crystalline samples along specific axes, and it was normalized with respect to the amorphous case. The substantial increase in photon yield (at 855 MeV) is illustrated by the ratio R, which compares the intensity spectrum for particles along axial orientation with that for particles in random orientations, as depicted in 5. The BGO crystal along $\langle 111 \rangle$ exhibits the highest peak enhancement, followed by PWO and CsI. CsI's lower enhancement is attributed to high mosaicity, hindering coherent interactions and radiation enhancement (Section 2.1, Fig. 2). PWO and BGO, with lower mosaicity, exhibit significant coherent effects and higher enhancements. The values of R exceed 1 even for 50 MeV and 100 MeV photons (Table 2). Peak enhancement values and energies for PWO and BGO, in the table, were calculated via Gaussian fitting, errors from the covariance matrix. CsI, with unfeasible Gaussian fitting, were obtained from the statistical bootstrap method. This approach yielded maximum values and associated errors, linking peak energy to bootstrap result and representing error through bin size. Bootstrap method was also used to compute 50 MeV and 100 MeV enhancement values, along with uncertainties.

5. Conclusions

Our examination of the crystal quality of the samples through HRXRD tests at ESRF exhibited a high crystalline quality for PWO and

Table 2
Table of peak enhancement values, E_{peak} refers to the energy at the maximum of the enhancement, shown in the R_{peak} column. Also the values of the enhancement are included for 50 and 100 MeV photons energy.

Sample	E_{peak} (MeV)	R_{peak}	$R_{50\ MeV}$	$R_{100\ MeV}$
PWO	22.2 ± 0.8	2.26 ± 0.02	1.94 ± 0.18	1.37 ± 0.18
BGO	11.6 ± 0.5	3.31 ± 0.02	2.51 ± 0.30	1.63 ± 0.30
CsI	15.3 ± 0.9	1.67 ± 0.01	1.58 ± 0.09	1.35 ± 0.09

BGO, making them suitable for coherent effect applications instead of CsI samples. Our research investigates the potential use of such materials as gamma emitters in crystal-based light sources, due to the enhancement of the emitted radiation when the beam is aligned along a specific axis. Our findings have implications for the advancement of gamma detectors with improved efficiency, specifically in specific orientations, due to the increased probability of pair production. Additionally, our study has provided proof supporting the feasibility of manufacturing compact electromagnetic calorimeters for particle and astroparticle physics. In these detectors, the amplification of bremsstrahlung for electrons and positrons and pair production by photons is strongly increased. As a consequence, the electromagnetic shower length experiences a drastic reduction under particular crystal orientations. These advancements not only lead to cost savings but also open exciting avenues in particle and astroparticle physics research.

Declaration of competing interest

The authors declare that they have no known competing financial interests or personal relationships that could have appeared to influence the work reported in this paper.

Funding

This work was supported by INFN CSN5 (OREO and MC-INFN projects) and the European Commission through the H2020-INFRAINNOV AIDAINNOVA (G.A. 101004761), H2020-MSCA-RISE N-LIGHT (G.A. 872196) and EIC-PATHFINDER-OPEN TECHNO-CLS (G.A. 101046458) projects. A. Sytov acknowledges support from the H2020-MSCA-IF-Global TRILLION (G.A. 101032975).

References

[1] M.L. Ter-Mikaelian, High-energy Electromagnetic Processes in Condensed Media, Wiley, New York, 1972.
[2] V. Baier, V. Katkov, V. Strakhovenko, Electromagnetic Processes at High Energies in Oriented Single Crystals, World Scientific, Singapore, 1998.
[3] M. Kumakhov, On the theory of electromagnetic radiation of charged particles in a crystal, Phys. Lett. A 57 (1) (1976) 17–18, http://dx.doi.org/10.1016/0375-9601(76)90438-2.
[4] V. Baryshevsky, I. Dubovskaya, A. Grubich, Generation of gamma-quanta by channeled particles in the presence of a variable external field, Phys. Lett. A 77 (1) (1980) 61–64, http://dx.doi.org/10.1016/0375-9601(80)90637-4.
[5] Bandiera, et al., Investigation on radiation generated by sub-gev electrons in ultrashort silicon and germanium bent crystals, Eur. Phys. J. C 81 (284) (2021) URL https://doi.org/10.1140/epjc/s10052-021-09071-2.
[6] L. Bandiera, et al., Investigation of the electromagnetic radiation emitted by sub-GeV electrons in a bent crystal, Phys. Rev. Lett. 115 (2015) 025504, http://dx.doi.org/10.1103/PhysRevLett.115.025504.
[7] L. Bandiera, et al., Broad and intense radiation accompanying multiple volume reflection of ultrarelativistic electrons in a bent crystal, Phys. Rev. Lett. 111 (2013) 255502, http://dx.doi.org/10.1103/PhysRevLett.111.255502.
[8] U. Wienands, et al., Channeling and radiation experiments at SLAC, Nucl. Instrum. Methods Phys. Res. B 402 (2017) 11–15, http://dx.doi.org/10.1016/j.nimb.2017.03.097.
[9] L. Bandiera, et al., Strong reduction of the effective radiation length in an axially oriented scintillator crystal, Phys. Rev. Lett. 121 (2018) 021603, http://dx.doi.org/10.1103/PhysRevLett.121.021603.
[10] L. Bandiera, et al., Crystal-based pair production for a lepton collider positron source, Eur. Phys. J. C 82 (2022) http://dx.doi.org/10.1140/epjc/s10052-022-10666-6.
[11] V. Guidi, L. Bandiera, V. Tikhomirov, Radiation generated by single and multiple volume reflection of ultrarelativistic electrons and positrons in bent crystals, Phys. Rev. A 86 (2012) 042903, http://dx.doi.org/10.1103/PhysRevA.86.042903.
[12] Camattari, et al., Silicon crystalline undulator prototypes: Manufacturing and x-ray characterization, Phys. Rev. Accel. Beams 22 (2019) 044701, http://dx.doi.org/10.1103/PhysRevAccelBeams.22.044701.
[13] R. Camattari, et al., Homogeneous self-standing curved monocrystals, obtained using sandblasting, to be used as manipulators of hard X-rays and charged particle beams, J. Appl. Crystallogr. 50 (1) (2017) 145–151, http://dx.doi.org/10.1107/S1600576716018768.
[14] A.V.S. Andrei Korol, Novel Lights Sources beyond Free Electron Lasers, Springer Cham, 2022, http://dx.doi.org/10.1007/978-3-031-04282-9.
[15] L. Bandiera, V. Haurylavets, V. Tikhomirov, Compact electromagnetic calorimeters based on oriented scintillator crystals, Nucl. Instrum. Methods Phys. Res. A 936 (2019) 124–126, http://dx.doi.org/10.1016/j.nima.2018.07.085.
[16] L. Bandiera, et al., A highly-compact and ultra-fast homogeneous electromagnetic calorimeter based on oriented lead tungstate crystals, Front. Phys. 11 (2023) http://dx.doi.org/10.3389/fphy.2023.1254020, URL https://www.frontiersin.org/articles/10.3389/fphy.2023.1254020.
[17] L. Bandiera, I. Kyryllin, C. Brizzolari, et al., Investigation on steering of ultrarelativistic $e^{\pm}$ beam through an axially oriented bent crystal, Eur. Phys. J. C 81 (238) (2021) URL https://doi.org/10.1140/epjc/s10052-021-09021-y.
[18] H.e.a. Backe, Planar channeling experiments with electrons at the 855 MeV Mainz Microtron MAMI, Nucl. Instrum. Methods Phys. Res. B 266 (2008) 3835–3851, http://dx.doi.org/10.1016/j.nimb.2008.05.012.
[19] A. Sytov, et al., Steering of Sub-GeV electrons by ultrashort Si and Ge bent crystals, Eur. Phys. J. C 77 (2017) 901, http://dx.doi.org/10.1140/epjc/s10052-017-5456-7.